SURFACE AND INTERFACE ANALYSIS
Surf. Interface Anal. 2004; **36**: 155–160
Published online in Wiley InterScience (www.interscience.wiley.com). DOI: 10.1002/sia.1675

SIA

Synthesis and magnetic properties of ε-cobalt nanoparticles

H. T. Yang,[1] Y. K. Su,[1,2] C. M. Shen,[1] T. Z. Yang[1] and H. J. Gao[1]*

[1] Nanoscale Physics and Devices Laboratory, Institute of Physics, Chinese Academy of Sciences, Beijing 100080, China
[2] Department of Chemistry, Lanzhou University, Lanzhou 730000, China

Received 18 September 2003; Accepted 17 October 2003

Monodisperse cobalt nanoparticles are synthesized via a high-temperature thermal decomposition method in the presence of oleic acid and triphenylphosphine. The as-synthesized nanoparticles are stable against further deep oxidation when they are kept in heptane (C_7H_{16}). Time-dependent XPS studies indicate that oxidation of the as-synthesized cobalt nanoparticles in air is slow. The valence change of cobalt from the nanoparticle sample is not observed after it is kept in heptane under air for 90 days. The cobalt nanoparticles have a β-manganese-type structure (also called ε-Co). Annealing the nanoparticles at 500 °C under Ar (95%) + H_2 (5%) converts these particles from ε-Co to fcc-Co. Two-dimensional and three-dimensional self-assembled superlattices of the passivated cobalt nanoparticles are formed by slow evaporation of the carrier solvent. The magnetic properties of the cobalt nanoparticles in different forms are compared, which provides helpful information on the magnetostatic interaction of the nanoparticles.

KEYWORDS: Co nanoparticles; XPS; oxidation

INTRODUCTION

Research on monodisperse magnetic nanoparticles has been an extremely active area owing to the potential applications of these particles in information data storage.[1–6] The size and shape specificity of nanoparticles naturally can serve as building blocks of the self-assembled passivated nanoparticles supperlattices or nanoparticles arrays.[7] In order to prepare monodisperse magnetic nanoparticles and obtain ordered two- or three-dimensional self-assembled superlattices, the nanoparticles need to be coated with organic surfactants to prevent them from irreversible aggregation.[8–10] Triphenylphosphine (TPP) was widely used in the synthesis of phosphine-stabilized gold or other metal nanoparticles.[11–15] The phenyl groups in TPP can provide greater steric hindrance than straight-chained alkyl groups such as tributyl and trioctyl to control the size of non-magnetic metal nanoparticles and to stabilize efficiently the magnetic nanoparticles. However, the synthesis of magnetic nanoparticles using TPP as a stabilizer has not been reported so far.[16]

In this article, we report on the synthesis of cobalt nanoparticles by thermal decomposition of cobalt carbonyl in the presence of TPP and oleic acid.[17,18] Both TPP and oleic acid are employed as stabilizers to control particle growth, to stabilize the particles and to prevent the particles from oxidation. X-ray photoelectron spectroscopy (XPS), x-ray diffraction (XRD) and infrared spectroscopy are employed to characterize the structure and surfactants of the cobalt nanoparticles. After the size of the cobalt nanoparticles is narrowed further through size-selective precipitation, two- and three-dimensional superlattice structures are obtained by controlled solvent evaporation. Magnetic measurement was conducted using MPMS-5 superconducting quantum interference device (SQUID) magnetometry.

*Correspondence to: H. J. Gao, Nanoscale Physics and Devices Laboratory, Institute of Physics, Chinese Academy of Sciences, Beijing 100080, China. E-mail: hjgao@aphy.iphy.ac.cn
Contract/grant sponsor: National Nature Science Foundation of China; Contract/grant number: 90101025; 90206028.

EXPERIMENTAL

The cobalt nanoparticles are synthesized by injecting the organometallic precursor into the surfactant mixture of TPP and oleic acid at 200 °C and keeping the growth temperature at 180 °C under an inert environment. Cobalt octacarbonyl [$Co_2(CO)_8$], TPP ($C_{18}H_{15}P$), oleic acid ($C_{18}H_{34}O_2$), dichlorobenzene ($C_6H_4Cl_2$) and heptane (C_7H_{16}) are obtained from ACROS Chemical. All the reagents are used as received without further purification. To synthesize 6–8 nm Co nanoparticles, a three-necked flask with 40 ml of dichlorobenzene is heated to ~220 °C under N_2 and stirred to eliminate the dissolved ambient air. Then 2.0 mmol of oleic acid and 2.0 mmol of TPP are added. In a separate reaction vessel, 2.0 mmol of $Co_2(CO)_8$ is combined with 5 ml of dry dichlorobenzene, warmed briefly to nearly 60 °C under N_2 until it is fully dissolved and finally injected rapidly into the flask. The solution turns black quickly and foams as $Co_2(CO)_8$ decomposes, nucleating Co nanoparticles and releasing gas. After the CO disappears, the black solution is refluxed at 185 °C for 20 min with vigorous stirring. Then

the black solution is cooled down to room temperature and a black precipitate appears by adding ethanol to the dispersion. The black precipitate is collected by centrifugation and washed with ethanol several times to remove excessive surfactant. The black magnetic precipitate is in turn redispersed in heptane and precipitated partially by slow titration of ethanol. Centrifuging the suspension isolates a precipitate enriched in large nanoparticles (30 wt.%) and leaves the small nanoparticles (70 wt.%) in the supernatant. Additional ethanol is added to the supernatant to isolate a second fraction of the small nanoparticles. Cobalt nanoparticles of average diameter 7 nm are obtained by a gentle destabilization/redispersion procedure with a size distribution (σ) of ~5%. When increasing the concentration of TPP and oleic acid by a factor of 2, cobalt nanoparticles of average diameter 5 nm can be formed.

X-ray photoelectron spectroscopy was used to examine the composition of the passivated cobalt nanoparticles. The Co $2p_{1/2}$ and Co $2p_{3/2}$ peaks of the cobalt nanoparticles coated with TPP and oleic acid were measured on an Escalab 5 spectrometer with monochromated Mg x-rays at 10 kV. The structure of the nanoparticles was examined using a Rigaku D/MAX 2400 x-ray diffractometer with Cu Kα radiation (λ = 1.5406 Å). Samples for XPS and XRD analysis were prepared by spreading several drops of cobalt dispersion on standard Si(111) wafers with a 150 nm thick SiO_2 layer and evaporating the solvent. A vacuum-transfer vessel was used to carry the sample from the drying box to the chamber without exposing the sample to the air. Infrared spectra of the samples were recorded using a Bruker Equinox 55 at room temperature by dropping the colloid solution on a KBr tablet. Transmission electron microscopy (TEM) (Jeol-200CX operating at 120 kV) and high-resolution TEM (HRTEM) (Philips CM200FEG operating at 200 kV) were employed to determine the particle size distribution and the crystalline structure. Samples were formed by drying a heptane or octane dispersion of cobalt nanoparticles on amorphous carbon-coated copper grids. Magnetic studies were conducted using a Quantum Design MPMS-5 SQUID. Measurements of isolated particle properties were carried out on the as-synthesized particles or on the samples by diluting the cobalt nanoparticle dispersions with wax. The ordered thin films (superlattices of nanoparticles) were prepared by evaporation of a heptane solution of nanoparticles on a highly oriented pyrolytic graphite (HOPG) substrate using a standard airless procedure.

RESULTS AND DISCUSSION

X-ray photoelectron spectroscopy is used for surface element analysis of the nanoparticles. In the XPS analysis, the penetration depth of the XPS beam is 3.0–5.0 nm but the chain length of oleic acid and TPP is <2.0 nm. The depth probed from the surface of the cobalt nanoparticles to the core of the cobalt nanoparticles is 1.0–3.0 nm, which ensures that the surface valence of the molecule-coated cobalt nanoparticles can be detected. Figure 1(a) is the XPS spectrum of the freshly prepared cobalt nanoparticles. Characteristic peaks of cobalt, carbon and phosphorus are

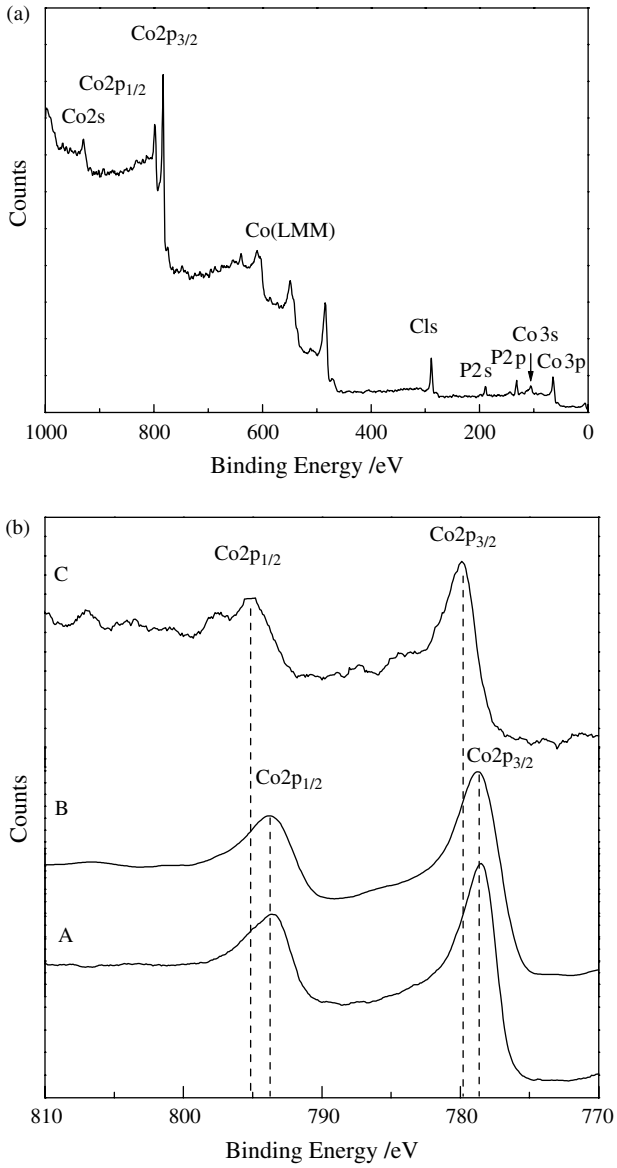

Figure 1. The XPS spectra of: (a) molecular coated cobalt nanoparticles; (b) Co 2p of the cobalt nanoparticles kept for 1 day (A), 90 days (B) and 120 days (C).

observed. Because cobalt is the only non-volatile product of the reaction $[Co_2(CO)_8] \rightarrow 2Co + 8CO$ and all the residual surfactant is removed by washing the precipitate with ethanol several times, the characteristic peaks of the carbon and the phosphorus are introduced from the TPP and oleic acid-coated surface of cobalt nanoparticles. According to the literature,[19] oleic acid and TPP should react or coordinate with the surface atoms of the Co nanoparticles to prevent oxidation or aggregation of the Co nanoparticles. Figure 1(b) is the XPS spectrum of the Co $2p_{3/2}$ and Co $2p_{1/2}$ peaks of the cobalt nanoparticles from a dispersion kept under air for 1 day (curve A), 90 days (curve B) and 120 days (curve C), respectively. The Co $2p_{3/2}$ and Co $2p_{1/2}$ peaks of the cobalt nanoparticles kept under air for 1 day are at 778.5 and 793.6 eV, respectively. The difference between the two peaks is 15.1 eV, which is consistent with the standard spectra of the element cobalt. X-ray photoelectron spectroscopy on cobalt nanoparticles kept in heptane under air for 90 days

shows the same Co $2p_{3/2}$ and Co $2p_{1/2}$ peaks from the typical valence state of Co^0, indicating that the Co nanoparticles in heptane are very stable against further oxidation. However, after it is kept in heptane under air for 120 days we observed a valency change of cobalt from the Co nanoparticle sample. The binding energies of Co $2p_{3/2}$ and Co $2p_{1/2}$ are now 779.9 and 795.4 eV, respectively, corresponding to the Co^{2+} oxidation state. Moreover, the peaks become broader and satellite peaks appear, which also indicates a change in the valency of the cobalt NPs.

The infrared spectra of free TPP, oleic acid and cobalt nanoparticles coated with oleic acid and TPP are shown in Fig. 2. By comparing the infrared spectra of the nanoparticles with free surfactants in Fig. 2 we can see that the organic molecules have indeed become a part of the nanoparticles. As shown in Fig. 2, peaks corresponding to C═O stretching at ~1710 cm^{-1} and 1285 cm^{-1}, P–Φ stretching at 1711 cm^{-1}, rocking and bending mode of the methylene group—$\omega(CH_2)$ at 1270 cm^{-1}, bending mode of the phenyl group—γ(═CH) at 742 cm^{-1} and δ (benzene ring) at 697 cm^{-1} can be seen clearly. The only difference among these characteristic peaks is either the peak intensity or a slight shift in the peak position. For example, the peak position of the longitudinal modes of oleic acid and TPP shifts to lower wavenumbers after TPP and oleic acid are adsorbed on the surface of the cobalt nanoparticles, appearing in the region 2925–2923 cm^{-1} for $\nu_a(CH_2)$, 2854–2852 cm^{-1} for $\nu_s(CH_2)$ and 2958–2955cm^{-1} for $\nu_s(CH_3$, ip). This is believed to be due to the organic molecules forming a relatively close-packed layer, thereby constraining their own mobility on the surface of the nanoparticles.[20–22] Thus, this steric constraint affects the transverse modes (rocking mode, wagging mode, etc.) more than the longitudinal modes (stretching mode, etc.). However, the peaks corresponding to the C═O stretching mode—ν(C═O) at 1710 cm^{-1} and 1285 cm^{-1} disappear in curve C but the P–Φ stretching mode—ν(P–Φ) at 1434 cm^{-1} still appears in curve C, although they both belong to a longitudinal mode because the C═O band position is the closest to the surface of the cobalt nanoparticles. From these results, a chemical bond can be formed between O and Co atoms and a coordinate bond between P and Co atoms on the surface of the nanoparticles. Thus, the C═O stretching mode disappears in the coated nanoparticles but the P–Φ stretching mode ν(P–Φ) at 1434 cm^{-1} is still visible in curve C of Fig. 2.

X-ray diffraction of 3 nm TPP–oleic acid-passivated Co nanoparticles shows a broad peak centred at $2\theta = 44.5°$, as shown in Fig. 3(a). As the particle size increases from 6 nm to 9.5 nm, the XRD pattern (Figs 3(b)–3(d)) can be indexed to a crystalline structure, the β-manganese phase

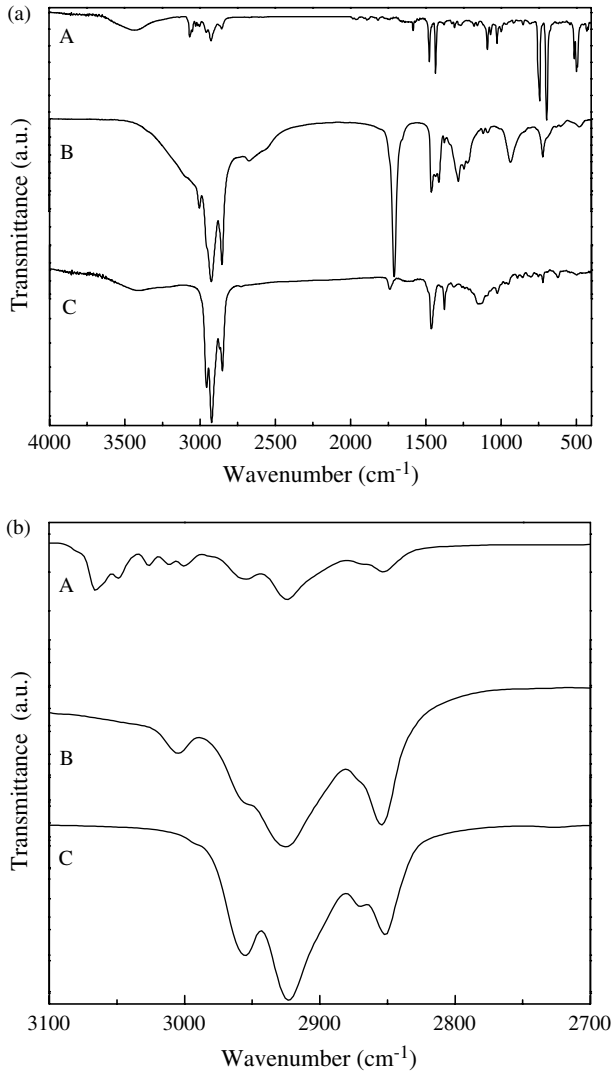

Figure 2. Infrared spectra of free TPP (curve A), free oleic acid (curve B) and cobalt nanoparticles coated by oleic acid and TPP (curve C). Spectrum (b) is the high magnification spectrum of that part of (a) with the wavenumber range 2700–3100 cm^{-1}.

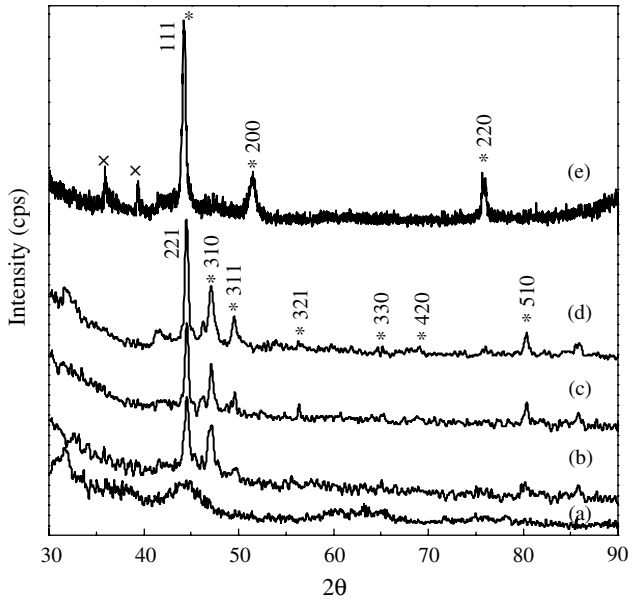

Figure 3. X-ray powder diffraction pattern of ε-Co nanoparticles passivated with $C_{18}H_{34}O_2/C_{18}H_{15}P$: (a) as-synthesized 3 nm particles; (b–d) as-synthesized particles of 6.5, 8.0 and 9.5 nm, respectively; (e) after annealing at 500 °C under Ar + H_2 (5%) for 3 h. Peaks corresponding to cobalt are denoted by *; peaks corresponding to CoO are denoted by ×.

(a high-temperature phase of manganese), and also to ε-Co, which is metastable.[23] After the sample of 6 nm ε-Co is annealed at 500 °C under Ar (95%) + H_2 (5%) for 3 h, it can transform completely to the fcc phase (Fig. 3(e)). Subsequent cooling does not convert the fcc structure back to its original ε-Co structure. This is in good agreement with the ε-Co structure change observed elsewhere.[24] In Fig. 3(e), the small diffraction peaks of the cobalt oxide (CoO) are observed after annealing. The average particle diameter can be estimated using Scherrer's formula.[25] The average sizes calculated from Figs 3(b)–3(e) are 6.5, 8.0, 9.5 and 27.3 nm, respectively, indicating the agglomeration and growth of the cobalt nanoparticles during annealing.

Slow evaporation of the heptane dispersion of cobalt nanoparticles spreading on a flat substrate allows the formation of well-organized superlattice structures. When the solution concentration is nearly 1%, the cobalt nanoparticles are self-assembled into well-defined and extended two-dimensional superlattices, as shown in Fig. 4. From the histogram of the size distribution and the TEM image, it can be seen that the particles are uniform. The average diameter of the nanoparticles is 7.2 ± 0.5 nm and the average spacing between neighbouring particles is 1.9 nm. Controlled evaporation of the octane dispersion of similar monodisperse cobalt nanoparticles at 40 °C leads to a three-dimensional superlattice structure. Figure 5 is the TEM image of the three-dimensional superlattice of ~5 nm cobalt nanoparticles. The ordered area in the superlattices extends over 0.6 μm × 0.6 μm. Both two- and three-dimensional superlattices have a hexagonal stacking structure. The HRTEM image of the cobalt nanoparticles, as shown in Fig. 5(c), reveals complicated interference patterns that are consistent with multiple crystalline orientations contained within a single nanocrystal.[26]

Magnetic properties of the ε-Co nanoparticles deposited on HOPG substrate are measured by SQUID using a standard airless procedure. The magnetization as a function of temperature in a 10 Oe field between 5 K and 300 K determines the blocking temperature using the zero-field cooling (ZFC) procedure. Figure 6 shows typical results for magnetic ε-Co nanoparticles of several different sizes below the critical size at which a particle becomes a single domain magnet and is small enough to display superparamagnetism.[27] From the concrete measurement data, the blocking temperature (T_b) of 6.5, 7.2, 8.0 and 9.5 nm Co nanoparticles is at 60, 92, 100 and 150 K, respectively. The blocking temperature increases as the size of ε-Co nanoparticles increases, which is consistent with the behaviour of fine particles. The broad transition from superparamagnetism to ferromagnetism shown in Fig. 6 at around T_b is probably due to the magnetostatic particle interactions in the close-packed arrays. The blocking

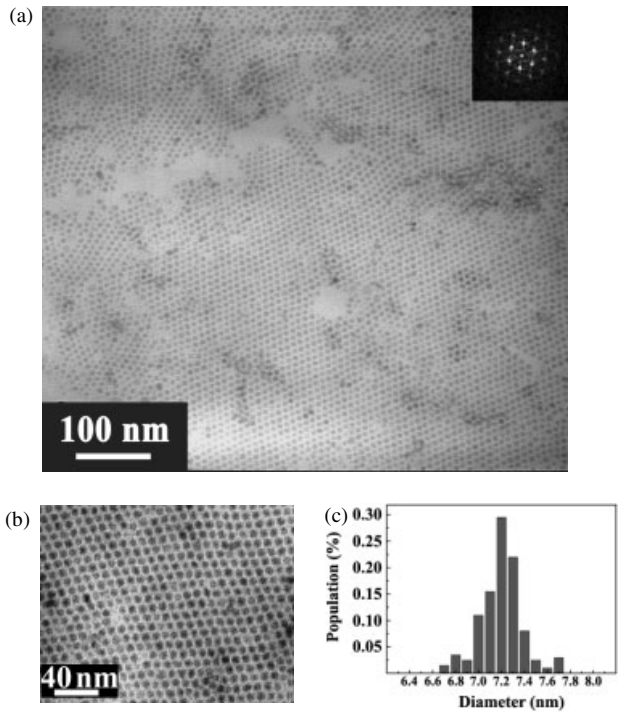

Figure 4. The TEM image of a two-dimensional superlattice of cobalt nanoparticles shown at low (a) and higher (b) magnification. The two-dimensional Fourier transform power spectrum of the image is inset in (a) and indexes into a hexagonal close-packed (hcp) structure. (c) A histogram of the size distribution shows that the average diameter of the nanoparticles is 7.2 ± 0.5 nm.

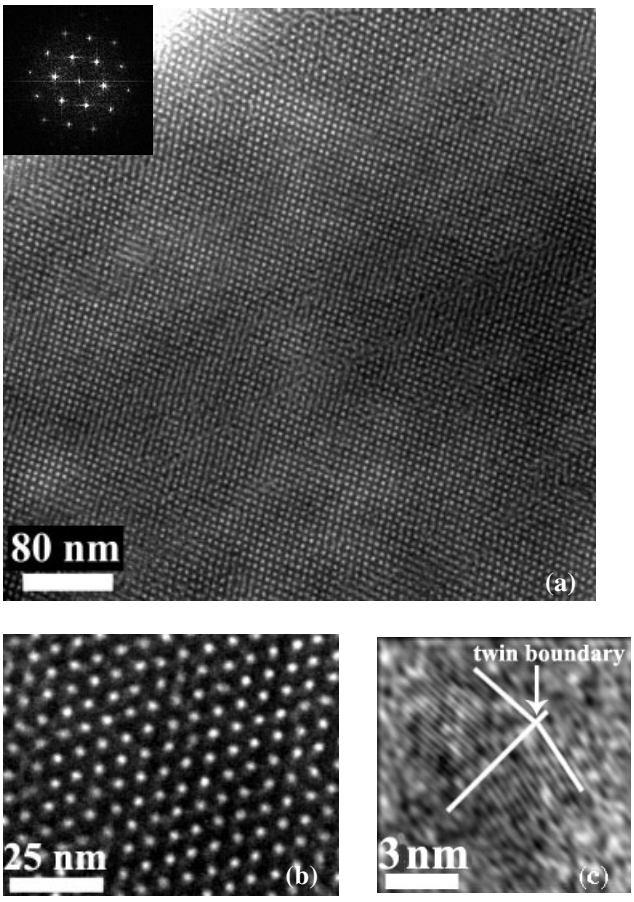

Figure 5. The TEM image of a three-dimensional superlattice of cobalt nanoparticles shown at low (a) and high (b) magnification. The Fourier transform power spectrum of the image is inset in (a). (c) The HRTEM image of a single particle with a twin structure.

temperature should roughly satisfy the relationship

$$T_b = KV/30k_b$$

where K is the anisotropy constant, k_b is Boltzmann's constant and V is the average volume of the particle. With knowledge of the blocking temperature and the particle size, the anisotropy constant of ε-Co nanoparticles of sizes 6.5, 7.2, 8.0 and 9.5 nm is 2.1×10^6, 1.9×10^6, 1.5×10^6 and 1.3×10^6 erg cm^{-3}, respectively. The result is smaller than that of bulk fcc cobalt (2.7×10^6 erg cm^{-3}).

Figure 7 shows the size-dependent magnetization (M) versus field (H) hysteresis loops at 5 K for ε-Co nanoparticles 6.5, 8.0 and 9.5 nm in diameter, respectively. The coercive field H_c of 6.5, 8.0 and 9.5 nm Co nanoparticles is 247, 386 and 838 Oe, respectively; H_c increases with increasing size of the cobalt nanoparticles, which is the behaviour of single-domain particles caused by thermal effects. Below the blocking temperature T_b, the magnetic moment of the nanoparticles is pinned along an 'easy' axis and is ferromagnetic. The energetic barrier pinning the magnetic moment of the nanoparticles and preventing its relaxation is proportional to the product of the anisotropy constant (K) and the volume of the nanoparticles (V). As the size of the nanoparticles decreases, the width of the hysteresis loop decreases with the decrease in KV. As the size of the ε-Co NPs decreases, the sharp drop in saturation magnetization (relative to that for bulk Co) results from the increase in the surface-to-volume ratio of the ε-Co nanoparticles.

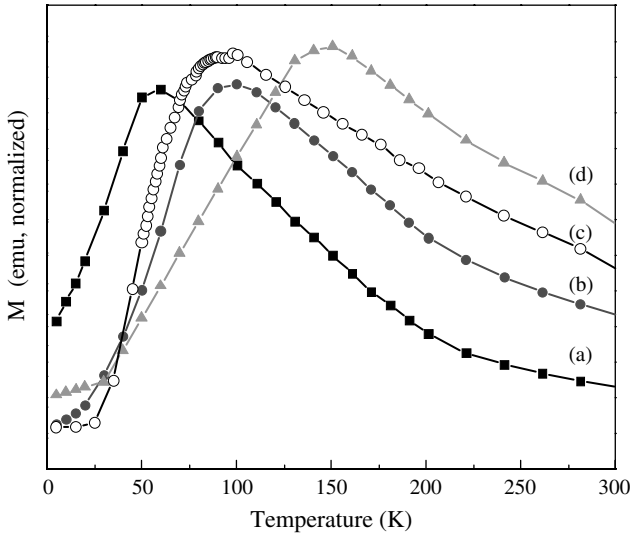

Figure 6. Zero-field cooling magnetization vs. temperature of 6.5, 7.2, 8.0 and 9.5 nm ε-Co nanoparticles showing blocking temperature (T_b): (a) 60 K; (b) 92 K; (c) 100 K; (d) 150 K.

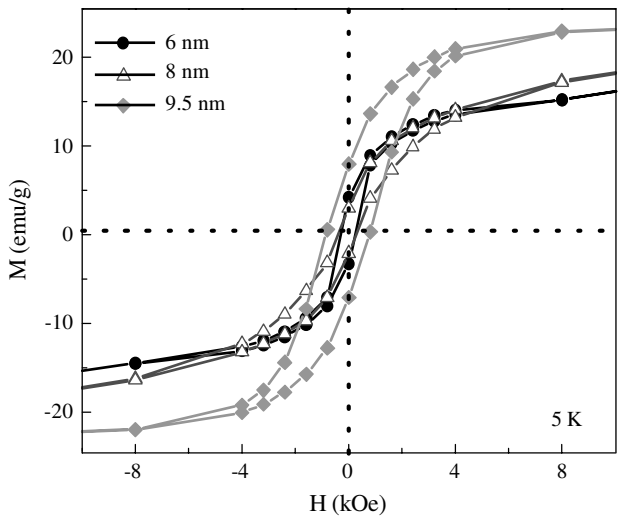

Figure 7. Magnetization versus field (M vs. H) hysteresis loops at 5 K for 6.5, 8 and 9.5 nm ε-Co nanoparticles samples. The coercive field H_c for 6.5, 8.0 and 9.5 nm Co nanoparticles, is 247, 386 and 838 Oe, respectively.

Figures 8(a) and 8(b) show the hysteresis loops of the cobalt nanoparticle powder compacted into a capsule made from bone powder at 250 and 10 K, respectively. Cobalt nanoparticles show no hysteresis in their magnetization data at 250 K, indicating a superparamagnetism behaviour at room temperature. Below the blocking temperature the cobalt nanoparticles are ferromagnetic. At 10 K, the remnant magnetization, (M_r) is ~1.5 emu g^{-1}, the coercive field (H_c) is 163 Oe and the magnetization at saturation (M_s) is estimated to be only 14.0 emu g^{-1} (the estimation is based on an extrapolation of curves of H/M versus H). Figure 8(c) shows the hysteresis loop for diluting particles with wax (a mass ratio of cobalt nanoparticles/wax = 1 : 4). There is a clear change in the shape of the hysteresis loop: M_r reaches 7.3 emu g^{-1}, M_s reaches 59.6 emu g^{-1} and H_c increases from 163 to 600 Oe in comparison with the isolated cobalt nanoparticle powder. Figure 8(d) shows the hysteresis loop of the ordered arrays of the cobalt nanoparticles on HOPG substrate: M_r reaches 12.6 emu g^{-1} and H_c increases to 790 Oe but the improvement in M_s (61.6 emu g)$^{-1}$ is not obvious in comparison with diluting particles with wax. These values (Table 1) are low compared with those obtained for the bulk phase. The observed changes cannot be attributed to the coalescence of the cobalt nanoparticles because TEM images

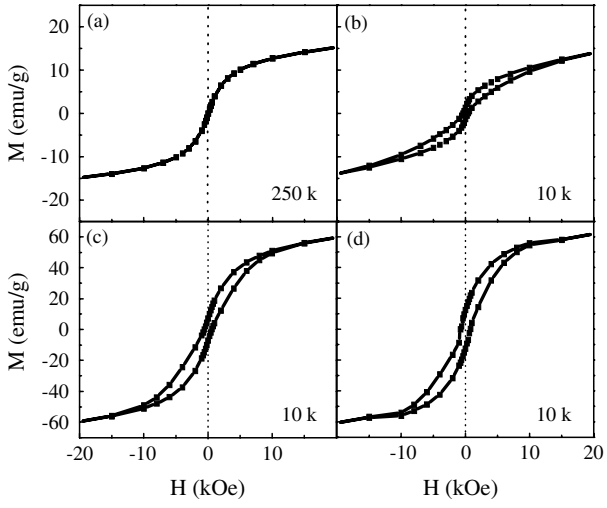

Figure 8. Hysteresis loop of powder of cobalt nanoparticles compacted into a capsule obtained at 250 K (a) and 10 K (b). (c) Cobalt nanoparticles diluted with wax. (d) Cobalt nanoparticles deposited on HOPG and dried under N_2 to prevent oxidation.

Table 1. Magnetic properties of cobalt nanoparticles in different physical states

Physical state	M_s (emu g^{-1})	M_r (emu g^{-1})	M_rM_s	H_c (Oe)
Powder in a capsule	14.0	1.5	0.11	163
Diluted particles with wax	59.6	7.3	0.12	600
On HOPG substrate	61.6	12.6	0.20	790

taken over large areas of the sample show no evidence of coalescence. The possible explanation for the change in magnetic properties is the exchange coupling between adjacent particles. The dipole coupling enhancement is attributed to the long-range order of the two-dimensional lattice and collective 'flips' of the magnetic dipoles.

CONCLUSIONS

Improved high-temperature thermal-decomposition synthetic routes to monodisperse cobalt nanoparticles have been presented. Growth and steric stabilization of the nanoparticles are controlled by a combination of oleic acid and TPP. The as-synthesized cobalt particles show very good ε-Co crystallinity and are stable in hydrocarbon solvent against air oxidation. The magnetic property of the ε-Co nanoparticles is found to be dependent on the size of the nanoparticles. The magnetic property of ordered arrays of the cobalt nanoparticles improves compared with those of cobalt nanoparticle powder compacted into a capsule or diluted with wax. These results are helpful for understanding the whole process of magnetic nanoparticle formation and for controlling the size distribution of the particles for further applications to spintronics.

Acknowledgements

The project is partly supported by the National Nature Science Foundation of China (Grant No's 90101025 and 90206028) and National '973' and '863' Projects of China.

REFERENCES

1. Zhang Z, Patel RC, Kothari R, Johnson CP, Friberg SE, Aikens PA. *J. Phys. Chem. B* 2000; **104**: 1176.
2. Peng X, Wickham J, Alivisatos AP. *J. Am. Chem. Soc.* 1998; **120**: 5343.
3. Valden M, Lai X, Goodman DW. *Science* 1998; **281**: 1647.
4. Link S, El-Sayed MA. *J. Phys. Chem. B* 1999; **103**: 8410.
5. He ST, Xie SS, Yao JN, Gao HJ, Pang SJ. *Appl. Phys. Lett*. 2002; **81**: 150.
6. Gao HJ, Sohlberg K, Xue ZQ, Chen HY, Hou SM, Ma LP, Fang XW, Pennycook SJ. *Phys. Rev. Lett*. 2000; **84**: 1780.
7. Wang ZL. *Aust. J. Chem*. 2001; **54**: 153.
8. Petit C, Talab A, Pileni MP. *J. Phys. Chem. B* 1999; **103**: 1805.
9. Puntes VF, Krishan Kannan M, Alivisatos AP. *Science* 2001; **291**: 2115.
10. Murray CB, Norris DJ, Bawendi MG. *J. Am. Chem. Soc.* 1993; **115**: 8706.
11. Schmid G, Pfeil R, Boese R, Bandermann F, Meyer S, Calis GHM, van der Velden JWA. *Chem. Ber*. 1981; **114**: 3634.
12. Feldheim DL, Grabar KC, Natan MJ, Mallouk TE. *J. Am. Chem. Soc.* 1996; **118**: 7640.
13. Clarke L, Wybourne MN, Brown LO, Hutchison JE, Yan M, Cai SX, Keana JFW. *Semicond. Sci. Technol*. 1998; **13**: A111.
14. Walter WW, Scott MR, Marvin GW, James EH. *J. Am. Chem. Soc.* 2000; **122**: 12 890.
15. Andres RP, Bein T, Dorogi M, Feng S, Henderson JI, Kubiak CP, Mahoney W, Osifchin RG, Reifenberger R. *Science* 1996; **272**: 1323.
16. Sun S. *8th IUMRS International Conference on Electronic Materials*, Xi'an, China, 10–14 June 2002; Abstr. Book, p. 382.
17. Murray CB, Sun SH, Gaschler W, Doyle H, Betley TA, Kagan CR. *IBM J. Res. Dev*. 2001; **45**: 47.
18. Dinega Dmitry P, Bawendi MG. *Angew. Chem. Int. Ed*. 1999; **38**: 1788.
19. Sun SH, Murray CB. *J. Appl. Phys*. 1999; **85**: 4325.
20. Ulan A. *An Introduction to Ultrathin Organic Films: From Langmuir–Blodgett to Self-Assembly*. Academic Press: Boston, 1991.
21. Korgel BA, Fullam S, Connolly S, Fitzmaurics D. *J. Phys. Chem. B* 1998; **102**: 8379.
22. He ST, Yao JN, Jiang P, Shi DX, Zhang HX, Xie SS, Pang SJ, Gao HJ. *Langmuir* 2001; **17**: 1571.
23. Shoemaker CB, Shoemaker DP, Hopkins TE, Yidepit S. *Acta Crystallogr. Sect. B* 1978; **34**: 3573.
24. Chen JM, Sorensen CM, Klabunde KJ, Hadjipanayis GC. *Phys. Rev. B* 1995; **51**: 11 527.
25. Klug HP, Alexander LE. *X-ray Diffraction Procedures for Polycrystalline and Amorphous Materials*. John Wiley: New York, 1962.
26. Marks LD. *Rep. Prog. Phys*. 1994; **57**: 603.
27. Leslie-Pelecky DL, Rieke RD. *Chem. Mater*. 1996; **8**: 1770.